J|A|C|S

A R T I C L E S

Synthesis, Crystal Structure, and Nonlinear Optical Properties of Li$_6$CuB$_4$O$_{10}$: a Congruently Melting Compound with Isolated [CuB$_4$O$_{10}$]$^{6-}$ Units

Shilie Pan,[†] Jared P. Smit,[†] Byron Watkins,[‡] Michael R. Marvel,[†] Charlotte L. Stern,[†] and Kenneth R. Poeppelmeier*,[†]

Contribution from the Department of Chemistry, Northwestern University, 2145 Sheridan Road, Evanston, Illinois 60208-3113, and Department of Physics and Astronomy, Northwestern University, 2145 Sheridan Road, Evanston, Illinois 60208-3112

Received May 11, 2006; E-mail: krp@northwestern.edu.

Abstract: Single crystals of Li$_6$CuB$_4$O$_{10}$ have been synthesized, and its crystal structure has been determined. Li$_6$CuB$_4$O$_{10}$ crystallizes in the non-centrosymmetric triclinic space group *P*1 (No. 1). The structure consists of isolated [CuB$_4$O$_{10}$]$^{6-}$ polyanions that are bridged by six LiO$_4$ tetrahedra. Li$_6$CuB$_4$O$_{10}$ is a congruently melting compound. It produces SHG intensity similar to that produced by KH$_2$PO$_4$ and is phase-matchable.

Introduction

A non-centrosymmetric structure is a prerequisite for crystals to exhibit efficient second-order nonlinear optical (NLO) effects that enable the manufacture of second-harmonic generating, electro-optical, and photorefractive devices.[1-7] A number of non-centrosymmetric compounds such as β-BaB$_2$O$_4$ (BBO), LiB$_3$O$_5$ (LBO), and KTiOPO$_4$ (KTP) are useful NLO materials for efficient second harmonic generation (SHG) of Nd:YAG lasers.[8-11] However, full use of these materials can be limited by optical imperfections (KTP), the incongruent nature of melting (LBO), or phase transitions (BBO). Therefore, much attention has been directed toward other non-centrosymmetric compounds as potential NLO materials during the past two decades and crystalline borates in particular.[12-19] Because most borate materials are incongruently melting compounds, it is difficult to grow large single crystals that are necessary for industrial applications.

As mentioned, borates are excellent NLO materials because planar ionic groups with π-conjugated systems such as BO$_3$ trigonal planes are responsible for the large SHG coefficients of these materials.[20] However, there are few non-centrosymmetric structures that contain only BO$_3$ units and even fewer that melt congruently.[21] Because the ternary Li$_2$O–CuO–B$_2$O$_3$ system has been unexplored largely,[22] new phases can provide interesting stoichiometries, structures, and properties. An extensive search for new borate phases in the Li$_2$O–CuO–B$_2$O$_3$ system has led to Li$_6$CuB$_4$O$_{10}$, a new congruently melting NLO material. In this paper, we report the synthesis, X-ray crystal structure, thermal analysis, and nonlinear optical properties of Li$_6$CuB$_4$O$_{10}$, containing isolated pseudosymmetric [CuB$_4$O$_{10}$]$^{6-}$ units.

Experimental Section

Solid-State Synthesis. Li$_6$CuB$_4$O$_{10}$ was discovered during a survey of the Li$_2$CO$_3$–CuO–H$_3$BO$_3$ system. It was synthesized by solid-state reactions from stoichiometric powder mixtures of Li$_2$CO$_3$ (99%, Sigma-Aldrich), CuO (99%, Sigma-Aldrich), and H$_3$BO$_3$ (99.99%, Alfa-Aesar). The mixtures were heated to 590 °C in air for 2–3 days with intermediate remixings. The sample purity was verified by X-ray powder diffraction.

X-ray powder diffraction analysis of Li$_6$CuB$_4$O$_{10}$ was performed at room temperature in the angular range of $2\theta = 10-70°$ with a scan step width of 0.02° and a fixed counting time of 1 s/step using an automated Rigaku X-ray diffractometer equipped with a diffracted-

[†] Department of Chemistry, Northwestern University.
[‡] Department of Physics and Astronomy, Northwestern University.

(1) Williams, D. J. *Angew. Chem. Int. Ed. Engl.* **1984**, *23*, 690.
(2) Zyss, J.; Oudar, J. L. *Phys. Rev.* **1982**, *26A*, 2028.
(3) Halasyamani, P. S.; Poeppelmeier, K. R. *Chem. Mater.* **1998**, *10*, 2753.
(4) Maggard, P. A.; Stern, C. L.; Poeppelmeier, K. R. *J. Am. Chem. Soc.* **2001**, *123*, 7742.
(5) Dalton, L. R.; Harper, A. W.; Wu, B.; Ghosn, R.; Laquindanum, J.; Liang, Z.; Hubbel, A.; Xu, C. *Adv. Mater.* **1995**, *7*, 519.
(6) Moerner, W. E.; Silence, S. M. *Chem. Rev.* **1994**, *94*, 127.
(7) Becker, P. *Adv. Mater.* **1998**, *10*, 979.
(8) Chen, C.; Wu, B.; Jiang, A.; You, G. *Sci. Sin.* **1985**, *B28*, 235.
(9) Chen, C.; Wu, Y.; Jiang, A.; You, G.; Li, R.; Lin, S. *J. Opt. Soc. Am.* **1989**, *B6*, 616.
(10) Liu, Y. S.; Dentz, D.; Belt, R. *Opt. Lett.* **1983**, *9*, 76.
(11) Hagerman, M. E.; Poeppelmeier, K. R. *Chem. Mater.* **1995**, *7*, 602.
(12) Wu, Y.; Sasaki, T.; Nakai, S.; Yokotani, A.; Tang, H.; Chen, C. *Appl. Phys. Lett.* **1993**, *74*, 7014.
(13) Aka, G.; Kahn-Harari, A.; Vivien, D.; Benitez, J.-M.; Salin, F.; Godard, J. *Eur. J. Solid State Inorg. Chem.* **1996**, *33*, 727.
(14) Chen, C.; Wang, Y.; Wu, B.; Wu, K.; Zeng, W.; Yu, L. *Nature* **1995**, *373*, 322.
(15) Chen, C.; Xu, Z.; Deng, D.; Zhang, J.; Wong, G. K. L.; Wu, B.; Ye, N.; Tang, D. *Appl. Phys. Lett.* **1996**, *68*, 2930.
(16) Hu, Z.; Higashiyama, T.; Yoshimura, M.; Mori, Y.; Sasaki, T. *J. Cryst. Growth* **2000**, *212*, 368.
(17) Sasaki, T.; Mori, Y.; Yoshimura, M.; Yap, Y. K.; Kamimura, T. *Mater. Sci. Eng.* **2000**, *R30*, 1.
(18) Wu, Y.; Liu, J.; Fu, P.; Wang, J.; Zhou, H.; Wang, G.; Chen, C. *Chem. Mater.* **2001**, *13*, 753.
(19) Pan, S.; Wu, Y.; Fu, P.; Zhang, G.; Li, Z.; Du, C.; Chen, C. *Chem. Mater.* **2003**, *15*, 2218.
(20) Chen, C.; Liu, G. *Annu. Rev. Mater. Sci.* **1986**, *16*, 203.
(21) Heller, G. *Top Curr. Chem.* **1986**, *131*, 42.
(22) Abdullaev, G. K.; Rza-Zade P. F.; Mamedov, Kh. S. *Russ. J. Inorg. Chem.* **1982**, *27*, 1037.

Table 1. Crystal Data and Structure Refinement for $Li_6CuB_4O_{10}$

empirical formula	$Li_6CuB_4O_{10}$
temp	153(2) K
fw	308.42
cryst syst	triclinic
space group	$P1$
unit cell dimensions	$a = 4.8131(6)$ Å $\alpha = 83.369(2)°$
	$b = 6.4288(8)$ Å $\beta = 71.623(2)°$
	$c = 7.0223(9)$ Å $\gamma = 73.364(2)°$
volume	197.50(4) Å^3
Z	1
density (calcd)	2.593 g/cm^3
absorption coefficient	2.808/mm
$F(000)$	147
cryst size	$0.02 \times 0.06 \times 0.14$ mm^3
θ range for data collection	3.06–28.70°
index ranges	$-6 \le h \le 6, -8 \le k \le 8, -9 \le l \le 9$
reflns collected/unique	1851/1592 [R(int) = 0.0145]
completeness to $\theta = 25.00$	99.7%
refinement method	full-matrix least-squares on F^2
data/restraints/params	1592/3/191
GOF on F^2	1.084
final R indices $[F_0^2 > 2\sigma(F_0^2)]^a$	R1 = 0.0546, wR2 = 0.1369
R indices (all data) ^{a}	R1 = 0.0625, wR2 = 0.1471
min. and max. transmission	0.76635, 0.94653
largest diff. peak and hole	2.24 and -0.96

^{a} R1 = $\Sigma||F_o| - |F_c||/\Sigma|F_o|$ and wR2 = $[\Sigma w(F_o^2 - F_c^2)^2/ \Sigma wF_0^4]^{1/2}$ for $F_0^2 > 2\sigma(F_0^2)$.

Table 2. Atomic Coordinates ($\times 10^4$) and Equivalent Isotropic Displacement Parameters (Å$^2 \times 10^3$) for $Li_6CuB_4O_{10}{}^a$

atom	Wyckoff position	x	y	z	U_{eq}
Li(1)	1a	4630(30)	6382(17)	2626(16)	10(2)
Li(2)	1a	5400(30)	1516(19)	2228(16)	10(2)
Li(3)	1a	−1470(40)	3350(30)	4420(30)	44(5)
Li(4)	1a	9630(40)	−1290(30)	3220(30)	40(4)
Li(5)	1a	−2550(50)	8670(30)	9520(40)	50(5)
Li(6)	1a	8830(50)	−440(40)	6640(30)	56(5)
Cu(1)	1a	7553(6)	3216(5)	8425(4)	25(1)
B(1)	1a	1200(30)	5370(20)	700(20)	7(3)
B(2)	1a	2700(30)	6100(30)	6860(30)	15(3)
B(3)	1a	3750(40)	1030(30)	6220(30)	17(3)
B(4)	1a	2100(30)	350(30)	9990(20)	11(3)
O(1)	1a	1090(20)	2048(17)	6037(14)	14(2)
O(2)	1a	9180(20)	1050(20)	121(16)	22(2)
O(3)	1a	4212(19)	4385(17)	740(14)	12(2)
O(4)	1a	5770(30)	5070(20)	6504(16)	38(3)
O(5)	1a	787(18)	6033(14)	8779(12)	8(2)
O(6)	1a	−1220(30)	5840(30)	2275(18)	34(3)
O(7)	1a	1690(20)	7060(18)	5337(15)	11(2)
O(8)	1a	3360(20)	−561(18)	1472(15)	18(2)
O(9)	1a	4480(20)	307(16)	8054(13)	12(2)
O(10)	1a	6270(20)	500(30)	4577(18)	31(4)

^{a} U_{eq} is defined as one-third of the trace of the orthogonalized U_{ij} tensor.

beamed monochromator set for Cu Kα ($\lambda = 1.5418$ Å) radiation. The experimental powder X-ray diffraction pattern of $Li_6CuB_4O_{10}$ is in agreement with the calculated data on the basis of the single-crystal data, suggesting that it is pure phase (Figures S1 and S2 in the Supporting Information).

Single-Crystal Growth. Small single crystals of $Li_6CuB_4O_{10}$ were grown in air. Mixtures with stoichiometric molar compositions of Li_6-CuB_4O_{10} were melted at 930 °C in a covered platinum crucible that was placed into a vertical, programmable temperature Molysili furnace. It was held at that temperature for 24 h, slowly cooled to 590 °C at a rate of 0.05 °C/min, and finally cooled to room temperature at a rate of 10 °C/min. High yields of clear, sub-millimeter-size, blue tabular crystals were separated from the melt. Crystals of suitable quality for X-ray diffraction were selected under an optical microscope.

X-ray Crystallographic Studies. The crystal structure of Li_6-CuB_4O_{10} was determined by single-crystal X-ray diffraction on a Bruker SMART-1000 CCD diffractometer using monochromatic Mo Kα radiation ($\lambda = 0.71073$ Å) and integrated with the SAINT-Plus program.[23]

All calculations were performed with programs from the SHELXTL crystallographic software package.[24] The structure was solved by direct methods. A face-indexed absorption correction was performed using the XPREP program, followed by the SADABS program;[25] equivalent reflections were then averaged. Final least-squares refinement is on F_0^2 with data having $F_0^2 \geq 2\sigma(F_0^2)$. The final difference Fourier synthesis may have shown maximum and minimum peaks at 2.24 (1.61 Å from Li(4)) and -0.96 e·Å^{-3} (0.89 Å from Cu(1)), respectively. The structure was checked for missing symmetry elements with PLATON.[26] Crystal data and structure refinement information are summarized in Table 1.

Final atomic coordinates and equivalent isotropic displacement parameters of the title compound are listed in Table 2. Selected interatomic distances and angles are given in Table S1 in the Supporting Information.

Vibrational Spectroscopy. IR spectroscopy was carried out with the objective of specifying and comparing the coordination of boron in $Li_6CuB_4O_{10}$. The mid-infrared spectrum was obtained at room temperature via a Bio-Rad FTS-60 FTIR spectrometer. The sample was mixed thoroughly with dried KBr (5 mg of the sample, 500 mg of KBr). The spectrum was collected in a range from 400 to 4000 cm^{-1} with a resolution of 1 cm^{-1}.

Differential Thermal Analysis. Differential thermal analysis (DTA) was performed under static air on a TA Instruments DSC 2910 differential scanning calorimeter. The sample and reference (Al_2O_3) were enclosed in Pt crucibles, heated from room temperature to 930 °C, and then cooled to room temperature at a rate of 10 °C/min.

Transmission Spectrum. The transmission spectrum was recorded on the powder sample at room temperature using a Cary 5000 UV–vis–NIR spectrophotometer and can be seen in Figure S3 in the Supporting Information. The powder sample was mixed with KBr in a 1:10 ratio of $Li_6CuB_4O_{10}$/KBr, and the KBr background was deducted. A wide transmission range is observed from 200 to 2000 nm with one absorption peak around 610 nm in the spectrum.

Second-Harmonic Generation Measurement. Powder SHG measurements were carried out on the $Li_6CuB_4O_{10}$ sample by means of the Kurtz–Perry method.[27] About 100 mg of powder was pressed into a pellet which was then irradiated with a pulsed infrared beam (100 ns, 15 mJ, 10 Hz) produced by a Q-switched Nd:YAG laser of wavelength 1064 nm. A 532 nm filter was used to absorb the fundamental and pass the visible light onto a photomultiplier. A combination of a half-wave achromatic retarder and a polarizer was used to control the intensity of the incident power, which was measured with an identical photomultiplier connected to the same high-voltage source. This procedure was then repeated using a standard nonlinear optical material, in this case microcrystalline KH_2PO_4 (KDP), and the ratio of the second-harmonic intensity outputs was calculated. Since the SHG efficiency of powders has been shown to depend strongly on particle size,[27,28] polycrystalline $Li_6CuB_4O_{10}$ was ground and sieved (Newark Wire Cloth Company) into distinct particle size ranges, <20, 20–38, 38–53, 53–75, 75–90, 90–105, 105–150, and 150–180 μm. KDP samples were ground and sieved into the same particle size ranges for comparison.

(23) *SAINT-Plus*, version 6.02A.; Bruker Analytical X-ray Instruments, Inc.: Madison, WI, 2000.
(24) Sheldrick, G. M. *SHELXTL*, Version 6.14; Bruker Analytical X-ray Instruments, Inc.: Madison, WI, 2003.
(25) *Bruker SMART*, Version 5.054, and *SADABS*, version 2.05; Bruker Analytical X-ray Systems, Inc.: Madison, WI, 2003.
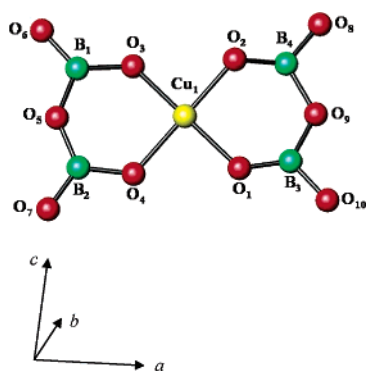(26) Spek, A. L. *J. Appl. Crystallogr.* **2003**, *36*, 7.

(27) Kurtz, S. Q.; Perry, T. T. *J. Appl. Phys.* **1968**, *39*, 3798.
(28) Dougherty, J. P.; Kurtz, S. K. *J. Appl. Crystallogr.* **1976**, *9*, 145.
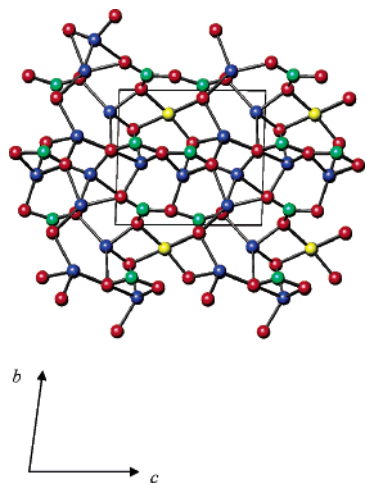
Figure 1. Drawing of the structure of Li$_6$CuB$_4$O$_{10}$ viewed down the *a* axis with the triclinic cell outlined. The blue spheres are Li, the yellow spheres are Cu, the green spheres are B, and the red spheres are O atoms.
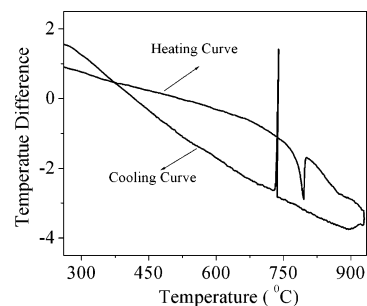

Figure 2. Structural unit [CuB$_4$O$_{10}$]$^{6-}$ in Li$_6$CuB$_4$O$_{10}$.

Results and Discussion

Crystal Structure. Li$_6$CuB$_4$O$_{10}$ crystallizes in the non-centrosymmetric triclinic space group *P*1. The structure is shown in Figure 1. Six unique lithium atoms, one unique copper atom, four unique boron atoms, and 10 unique oxygen atoms are in the asymmetric unit. The basic building units of the title compound are corner-shared BO$_3$ polyhedra that form isolated pyroborate (B$_2$O$_5$) units, and therefore, Li$_6$CuB$_4$O$_{10}$ can be written as Li$_6$Cu(B$_2$O$_5$)$_2$. The extended framework of the structure can be described as isolated pseudosymmetric [CuB$_4$O$_{10}$]$^{6-}$ units that are linked by LiO$_4$ polyhedra. The isolated [CuB$_4$O$_{10}$]$^{6-}$ unit is depicted in Figure 2. The CuO$_4$ polyhedra are nearly square planar, and the Cu–O bonds range from 1.883(12) to 2.008(10) Å. The CuO$_4$ polyhedra share four oxygen atoms with four boron atoms within two different B$_2$O$_5$ pyroborate groups (Figure 2). Because the [CuB$_4$O$_{10}$]$^{6-}$ polyanions are isolated in the structure, there is no interaction between the Cu^{2+} ions, and the linear temperature dependence of the reciprocal susceptibility for Li$_6$CuB$_4$O$_{10}$ accurately follows the Curie–Weiss law (Figure S4 and Table S3 in the Supporting Information).

The average Cu–O distance of 1.940(11) Å is similar to values observed in other copper borates such as Cu$_3$B$_2$O$_6$ and CuB$_2$O$_4$.[29,30] Likewise, the average Li–O distance compares

(29) Behm, H. *Acta Crystallogr.* **1982**, *38B*, 2781.
(30) Martinez-Ripoll, M.; Martinez-Carrera, S.; Garcia-Blanco, S. *Acta Crystallogr.* **1971**, *27B*, 677.

Figure 3. DTA curve of Li$_6$CuB$_4$O$_{10}$ recorded at a heating rate of 10 °C/min. The large difference between the heating and cooling peaks is due to supercooling of the melt.

well with the average Li–O distances in Li$_2$CuO$_2$[31] and LiB$_3$O$_5$,[32] and the average B–O distance compares to similar interactions observed in a variety of other borates.[21,33] The oxygen coordination varies from two-coordinate (O(4) and O(5)) to four-coordinate (O(1), O(2), O(3), O(6), O(7), and O(9)) to five-coordinate (O(8) and O(10)) (Table S2 in the Supporting Information).

The bond valence sums of each atom in Li$_6$CuB$_4$O$_{10}$ were calculated[34,35] and are listed in Table S2 in the Supporting Information. These valence sums agree with the expected oxidation states.

After review and during revision of this manuscript, the authors became aware of an unpublished report of Li$_6$CuB$_4$O$_{10}$.[36] Interestingly, the structure observed was centrosymmetric and Z = 3, with one centric and two acentric [CuB$_4$O$_{10}$]$^{6-}$ individual units. It is likely that there are other phases with this stoichiometry possible containing these [CuB$_4$O$_{10}$]$^{6-}$ units.

Vibrational Spectroscopic Characterization. The spectrum exhibited the following absorptions which were assigned referring to literature (Figure S5 in the Supporting Information).[37-39] The main infrared absorption region between about 1100–1400 cm^{-1} reveals several absorption bands owing to asymmetric stretching of trigonal BO$_3$ (1366, 1330, and 1175 cm^{-1}) groups. The bands at 710 and 675 cm^{-1} are the out-of-plane bending of B–O in BO$_3$. In the long-wavelength part of the spectrum, there are weak bands at 540 cm^{-1} which correspond to the deformation vibrations of trigonal BO$_3$ groups.

Thermal Stability. Figure 3 presents the DTA curve of Li$_6$CuB$_4$O$_{10}$. It shows one endothermic peak at 794 °C on the heating curve and one exothermic peak on cooling (supercooled) at 739 °C, which suggests that Li$_6$CuB$_4$O$_{10}$ melts congruently at 794 °C. To further verify that Li$_6$CuB$_4$O$_{10}$ melts congruently, 0.5 g of Li$_6$CuB$_4$O$_{10}$ powder was packed into a platinum crucible, heated to 930 °C, and then rapidly cooled to room temperature. Analysis of the powder XRD pattern of the solidified melt revealed that the entire solid product exhibited a diffraction pattern identical to that of the initial Li$_6$CuB$_4$O$_{10}$ powder, shown in Figure S6 in the Supporting Information,

(31) Weller, M. T.; Lines, D. R. *J. Solid State Chem.* **1989**, *82*, 21.
(32) Koenig, H.; Hoppe, R. *Z. Anorg. Allg. Chem.* **1978**, *439*, 71.
(33) Keszler D. A.; Sun, H. *Acta Crystallogr.* **1988**, *44B*, 1505.
(34) Brown, I. D.; Altermatt, D. *Acta Crystallogr*, **1985**, *41B*, 244.
(35) Brese, N. E.; O'Keeffe, M. *Acta Crystallogr.* **1991**, *47B*, 192.
(36) Sparta, K. Structural investigation of quaternary copper oxides with low dimensional magnetic properties. Ph.D. thesis, Institut für Kristallographie of the RWTH-Aachen, Aachen, Germany, 2003.
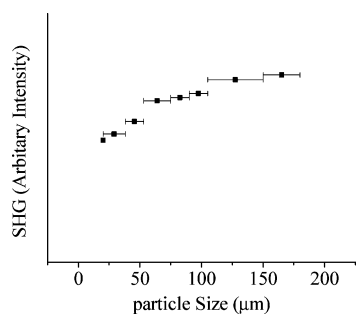(37) Li, J.; Xia, S.; Gao, S. *Spectrochim. Acta* **1995**, *51A(4)*, 519.
(38) Ross, S. D. In *The Infrared Spectra of Minerals*; Farmer, V. C., Ed.; Adlard, Dorking: Surrey, 1974; p 205.
(39) Liu, Z.; Li, S.; Zuo, C. *Thermochim. Acta* **2005**, *433*, 196.

Figure 4. Phase-matching, i.e, particle size vs SHG intensity, data for $Li_6CuB_4O_{10}$.

Figure 5. B_2O_5 pyroborate group. The green spheres are B, and the red spheres are O atoms. The two B atoms of the B_2O_5 dimer are aligned to show that the oxygen atoms are displaced from the plane.

further demonstrating that $Li_6CuB_4O_{10}$ is a congruently melting compound. The DTA curve of the solidified melt is shown in Figure S7 in the Supporting Information. Again, one endothermic peak at 794 °C is observed upon heating and one exothermic peak is observed upon cooling, further indicating that no other phases were present in the solidified melt. Therefore, large crystals of $Li_6CuB_4O_{10}$ can, in principle, be grown from stoichiometric melts.

Nonlinear Optical Properties. One preliminary measurement of second-order nonlinear optical effects for the powder sample of the title compound has been carried out by the Kurtz–Perry method at room temperature. The investigation probes properties associated with the determined symmetry group, in particular, the lack of an inversion center. The intensity of the green light (frequency-doubled output: $\lambda = 532$ nm) produced by the triclinic $Li_6CuB_4O_{10}$ crystal powder is similar to that of KDP powder, indicating that $Li_6CuB_4O_{10}$ has a powder SHG effect similar to that of KDP. The SHG signal provides a highly sensitive and definitive test for the absence of a center of symmetry in the compound. In addition, $Li_6CuB_4O_{10}$ was found to be phase-matchable (Figure 4). As the particle size of $Li_6CuB_4O_{10}$ becomes significantly larger than the coherence length of the material, the SHG intensity is independent of particle size.[27,28]

According to the anionic group theory of nonlinear optical activity in borates,[20,40,41] the contribution of the borate groups to the SHG effect can be predicted qualitatively, where the planar ionic groups with π-conjugated systems such as BO_3 trigonal planes are responsible for the large SHG effects. However, changes in the alignment of the BO_3 constituent groups in the crystal structure will reduce the SHG effects.[20,40–42] Although the central $[CuB_4O_{10}]^{6-}$ polyanion appears to have a center of symmetry, it is acentric, and therefore, $Li_6CuB_4O_{10}$ adopts the non-centrosymmetric space group $P1$. All of the Cu–O bonds in the CuO_4 polyhedra are different lengths. Each of the four boron atoms surrounding the central copper atom
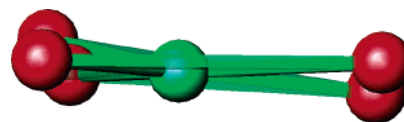
are on unique crystallographic sites, and each BO_3 polyhedron contains three different B–O bond lengths with various distortions. Additionally, none of the BO_3 groups are in the same plane (Table S1 in the Supporting Information). The structural arrangement for the BO_3 groups in $Li_6CuB_4O_{10}$ are not aligned in the same directions, and the two corner-shared BO_3 groups of the B_2O_5 dimers are not planar (Figures 1 and 5), which does lead to some cancellation of the microscopic hyperpolarizability coefficients. However, because these cancellations are limited, the intensity of the SHG light produced by $Li_6CuB_4O_{10}$ powder is similar to that produced by KDP powder. Efforts are currently underway to grow large crystals of $Li_6CuB_4O_{10}$ and to measure a more complete set of nonlinear optical properties.

Conclusions

$Li_6CuB_4O_{10}$ has been synthesized, and its structure has been determined by single-crystal X-ray diffraction. The structure consists of isolated $[CuB_4O_{10}]^{6-}$ polyanions that are bridged by six LiO_4 tetrahedra. Because $Li_6CuB_4O_{10}$ lacks a center of symmetry, it exhibits distinct nonlinear optical properties which are similar to those of KDP powder and is also phase-matchable. $Li_6CuB_4O_{10}$ melts congruently which suggests that large single crystals of $Li_6CuB_4O_{10}$ can be grown from a liquid of the same composition.

Supporting Information Available: An X-ray crystallographic file in CIF format including crystallographic details, interatomic distances and angles, calculated X-ray diffraction pattern data, observed X-ray diffraction pattern data of $Li_6CuB_4O_{10}$ before and after melting, DTA curve of the solidified melt of $Li_6CuB_4O_{10}$, the infrared spectrum, and the linear temperature dependence of the reciprocal susceptibility for $Li_6CuB_4O_{10}$. This material is available free of charge via the Internet at http://pubs.acs.org.

JA0633114

(40) Chen, C.; Wu, Y.; Li, R. *Int. Rev. Phys. Chem.* **1989**, *8*, 65.
(41) Chen, C.; Wu, Y.; Li, R. *J. Cryst. Growth* **1990**, *99*, 790.
(42) Xia, Y. *Adv. Mater.* **1994**, *6*, 510.